Conical dynamics of Bessel beams

Article *in* Optical Engineering · July 2007

DOI: 10.1117/1.2752167

4 authors, including:

Marcelino Anguiano-Morales
Instituto Tecnológico de Chihuahua
35 PUBLICATIONS **104** CITATIONS
SEE PROFILE

Marcelo David Iturbe-Castillo
Instituto Nacional de Astrofísica, Óptica y Elect…
150 PUBLICATIONS **1,221** CITATIONS
SEE PROFILE

S. Chávez-Cerda
Instituto Nacional de Astrofísica, Óptica y Elect…
143 PUBLICATIONS **2,419** CITATIONS
SEE PROFILE

Conical dynamics of Bessel beams

Marcelino Anguiano-Morales
M. Maribel Méndez-Otero
Postgrado en Optoelectrónica
FCFM, BUAP
C.P.72570, Apdo. Postal 1152
Puebla, Pue. México
E-mail: anguiano@fcfm.buap.mx

M. David Iturbe-Castillo
Sabino Chávez-Cerda, MEMBER SPIE
Instituto Nacional de Astrofísica
Óptica y Electrónica
C. P.7200, Apdo. Postal 51 y 216
Puebla, Pue. México

Abstract. We present an analysis of the dynamics of conical waves partially obstructed by opaque objects. The analysis yields the incoming and outgoing conical waves that form the Bessel beams (or any other propagation-invariant beams) when opaque obstructions are set on and off axis. The results show that the invariance of Bessel beams with finite transverse extension is no longer maintained under the mentioned conditions.
[DOI: 10.1117/1.2752167]

Subject terms: Bessel beams; diffraction-free beams; axicon optics.

Paper 060505R received Jun. 26, 2006; revised manuscript received Dec. 8, 2006; accepted for publication Jan. 8, 2007; published online Jul. 2, 2007.

1 Introduction

It is well known that real Bessel beams have the property of propagating without spreading or changing their shape for considerable distances. An even more interesting property is that, when the beam is partially blocked, it self-reconstructs after some distance. These intriguing properties have been observed[1–4] and exploited in multiple applications.[3,5–13] In the first attempts to explain the self-reconstruction of Bessel beams, diffraction theory was used, assuming that the reconstruction was related to the Arago spot.[14] Since then, many other groups have investigated this phenomenon and used different approaches to explain it, for instance, using Babinet's principle.[8]

In particular, J_0-Bessel beams were first expressed by Durnin, using a reduced form of the Whittaker integral that represents the superposition of plane waves whose wave vectors lie on the surface of a cone.[5] This interpretation has been widely accepted in the literature. However, we observe that the J_0-Bessel beams' phase fronts are ringed plane waves with π phase jumps.

Later on, a new formalism based on traveling waves was introduced to explain the nature of Bessel beams.[13–15] This approach is more rigorous in that it requires that the solutions of the Helmholtz equation satisfy fundamental theorems related to propagating waves. The result of this approach was that Bessel beams are due to the superposition of two kinds of conical traveling waves expressed in terms of the Hankel functions representing incoming and outgoing conical waves. The inherent singularity of these functions was physically explained.[14,16] The relevance of the conical-wave approach is that it helped to easily understand the apparently odd features of Bessel beams. Even more, by combining the Whittaker integral and the conical-wave approach it was possible to demonstrate new families of nondiffracting beams governed by the Helmholtz equation.[17–19] Although the conical features of Bessel beams are commonly mentioned in the literature, the propagation of conical waves has never been investigated.

In this work we present a thorough study of the dynamics of the conical waves that compose the nondiffracting J_0-Bessel beam. The propagation of incoming and outgoing conical waves is investigated when they are partially obstructed by opaque objects, on and off axis. The results are used to explain the reconstruction properties of Bessel beams under the same conditions. We also present experimental results for Bessel beams obstructed off axis that corroborate the theoretical results.

2 Theoretical Analysis of the Self-Reconstruction

It is widely known that any electromagnetic field $U(x,y,z)$ related to the Helmholtz wave equation that has the property of being nondiffracting can be expressed in terms of a reduced form of the Whittaker integral[17–20]

$$U(x,y,z) = \exp(ik_z z)\int_{-\pi}^{\pi} A(\varphi)\exp[ik_r(x\cos\varphi + y\sin\varphi)]\mathrm{d}\varphi, \tag{1}$$

where $A(\varphi)$ is a complex function corresponding to the frequency spectrum that lies on a ring of radius k_r in the frequency space. The components of the transverse and longitudinal wave vectors satisfy the relation $k^2=k_r^2+k_z^2$, where $k=2\pi/\lambda$ is the magnitude of the wave number and λ the wavelength of the field. Looking at the form of the integrand, we notice that its kernel is formed by plane waves in the polar direction defined by (φ,θ) (in spherical coordinates), where the angle θ is given by $\theta=\tan^{-1}(k_r/k_z)$. The field $U(r)$ then is composed by the continuous superposition of these plane waves whose wave vectors lie on the surface of the cone with vertex angle θ, and they are modulated by the spectral function $A(\varphi)$.

The continuous superposition of plane waves results in conical waves as shown in Fig. 1. Here we emphasize that the cone of wave vectors comprises simultaneously two conical waves, one incoming and the other outgoing. The incoming conical wave (ICW) can be represented by a Hankel function of the second kind, and the outgoing conical wave (OCW) by a Hankel function of first kind.[13,14] Notice that on propagation the ICW transforms into OCW

0091-3286/2007/$25.00

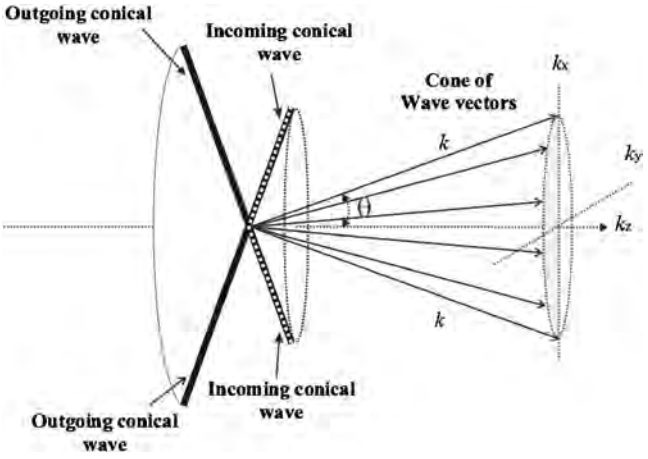

Fig. 1 Graphical representation of the Whittaker integral.

(see Fig. 2). The latter wave is the Green function of the Helmholtz equation and satisfies the Sommerfeld radiation condition; Bessel functions of the first kind, J_n, do not satisfy either of these conditions. In the literature on nondiffracting beams very little or nothing is discussed about the existence of either kind of conical waves. Propagation-invariant beams require both kinds to exist. This has also been rigorously demonstrated for other families of nondiffracting beams.[13,14,17,18]

Finite approximations to the conical waves represented in Fig. 1 can be created using different experimental configurations. The two most simple and common arrangements are shown in Fig. 2. In the first case, Fig. 2(a), an annular mask with a lens placed at the focal distance allows one to obtain Bessel beams when the mask is illuminated with a plane wave. In the second case, Fig. 2(b), a positive axicon generates a Bessel transverse intensity distribution when illuminated by a plane wave. In both configurations the ICWs carry energy to the optical axis and the OCWs carry this energy away from the axis. In a propagation-invariant beam both waves superpose and the former is the source of the latter, eliminating the singularity that appears in their mathematical description with the Hankel functions:

$$H_0^{(1)}(k_r r)\exp(ik_z z) = [J_0(k_r r) + iN(k_r r)]\exp(ik_z z) \tag{2}$$

and

$$H_0^{(2)}(k_r r)\exp(ik_z z) = [J_0(k_r r) - iN(k_r r)]\exp(ik_z z), \tag{3}$$

where $H_0^{(1)}(k_r r)$ and $H_0^{(2)}(k_r r)$ are the zero-order Hankel functions of the first and second kind, respectively, and $J_0(k_r r)$ and $N(k_r r)$ the zero-order Bessel and Newman functions of the first and second kind, respectively. Observe that plane waves whose wave vectors lie on a cone can also be obtained from a negative axicon; however, the resulting pattern will not be propagation-invariant, but will be a pure diffracting outgoing conical wave. As mentioned, for the formation of propagation-invariant optical beams (parabolic, Mathieu, or Bessel beams), a necessary condition is the superposition of ICWs and OCWs.

Within the region of existence of the Bessel beam, locally the light is traveling parallel to the optical axis, since instantaneously it is a transverse stationary wave in space. However, the energy flux follows the direction dictated by the cone of wave vectors for both the ICW and the OCW; see Fig. 2. This is the real reason for the reconstruction of an obstructed Bessel beam; the light is in fact coming from a region that was not obstructed by the opaque object. After passing through the optical axis the ICW generates the OCW and interferes with it to create the Bessel beam. However, prior to the predicted reconstruction, within the geometric shadow there is the appearance of light due to the edge waves at the obstruction. When the obstruction is circular and placed on axis, the edge waves are in a ring of negligible width (a delta) that creates a diffracting Bessel transverse intensity pattern whose features are not related with the impinging Bessel beam. This diffracting Bessel pattern is what is known as the Poisson or Arago spot.[21] The spot always appears at the same position, irrespective of whether the obstruction is illuminated with a plane wave, a focusing or defocusing wave, or an ICW or OCW, as is shown below.

3 Numerical Investigation of the Dynamics of Conical Waves

The numerical propagation of conical waves was performed by solving the Helmholtz equation using a non-

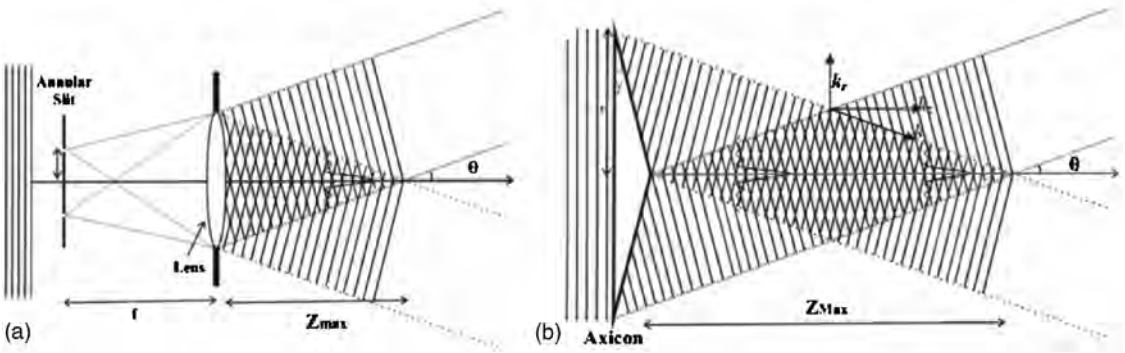

Fig. 2 Typical experimental configurations for the generation of Bessel beams: (a) annular mask and positive lens, and (b) an axicon.

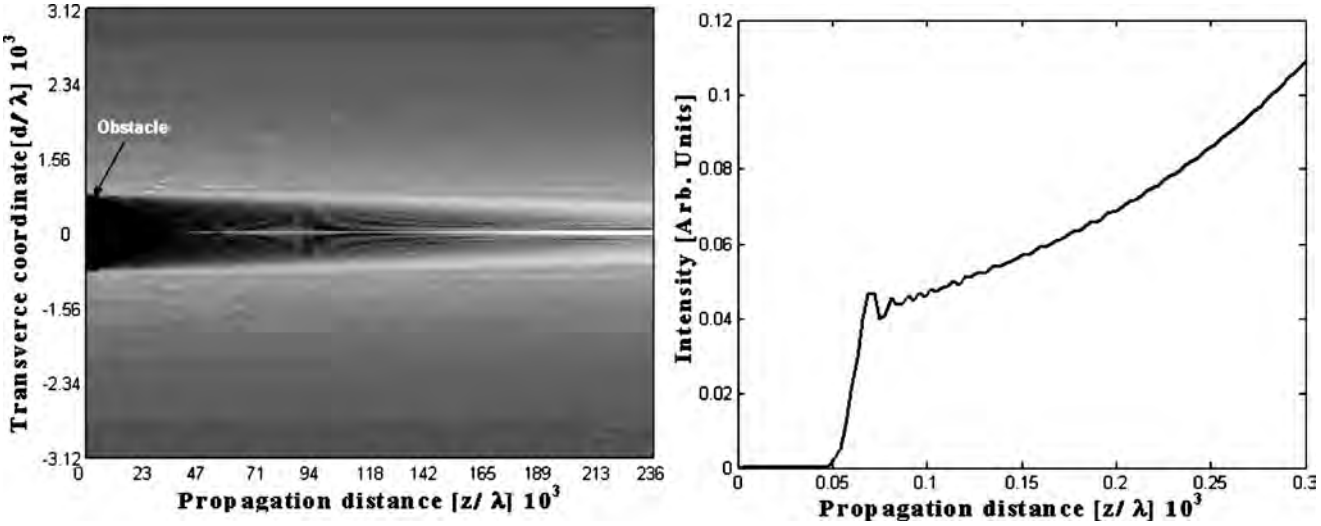

Fig. 3 Evolution of an ICW partially obstructed on axis, in the (x,z) plane, and behavior of the intensity on axis of the blocked beams.

paraxial beam propagation method. As special case we analyzed the effect of a circular opaque object that is partially blocking a conical wave. The zero-order Hankel functions, Eq. (2) and (3), were used as initial conditions of the conical waves. The angle of the conical wave considered was $\theta=4\times10^{-3}$ (radians), and the radius of the circular opaque obstruction was 8×10^{2} wavelengths. In the case of an ICW and when the object was set on axis (that is, on the z axis), the dynamics was the following: The shadow of the object shrank until it reached a minimum size. Geometrically, it should be a conical shadow. However, due to diffraction, within this region we observe the appearance of light, the edge waves creating the Arago spot; see Fig. 3. Within the shadow region after the appearance of the Arago spot, the intensity on axis grows until the vertex of the conic shadow, where the creation of a Bessel beams starts. After this point the intensity oscillates around a constant value.

When the obstruction was set off axis, the dynamics of the obstructed ICW was rather complex; see Fig. 4. We can observe that the shadow of the obstruction moved towards the axis and did not keep the symmetry of the object (as reference, the white circle represents the position and size of the obstruction). Initially, the shadow takes the shape of a lemniscate, reducing in size as it travels transversely through the propagation axis, after which it appears as a low-contrast shadow. Notice that as the ICW passes the axis it transforms into an OCW, and then a set of rings appears due to the interference of the ICW and the OCW that are creating the Bessel beam. In the last image, Fig. 4(d), when the characteristic rings of the Bessel distribution are formed, two low-contrast shadows on opposite sides of the center affect the uniform intensity of some rings. With further propagation the left-traveling shadow passed through the axis, merged with the right shadow (increasing its size), and continued traveling outwards.

In the case of an OCW and when the object was set on axis, the shadow of the object always grew; see Fig. 5. Near the optical axis one again finds the Arago spot; note that it appears at the same distance as in the case of the ICW. The on-axis intensity reached a maximum and then began to decay. When the object was set off axis, its shadow moved away from the optical axis, a well-known change of curvature was observed in the part of the shadow next to the axis, due the direction of the wave vectors in that region. The divergence of the shadow was clear in the vertical direction and the left direction of the transverse intensity distribution; see Fig. 6. Because the obstruction was placed to the left of the optical axis of the OCW, it is clear why the shadow should move to left. We notice that at the center of the whole pattern another circular shadow appeared; this is due

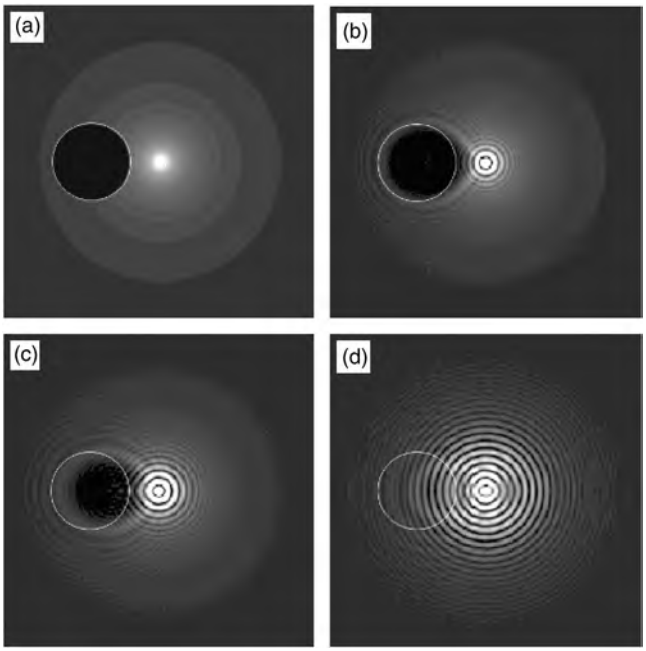

Fig. 4 Dynamics of an ICW partially obstructed off axis. Distance from the obstruction: (a) $1.5\times10^{4}\lambda$, (b) $4.7\times10^{4}\lambda$, (c) $9.4\times10^{4}\lambda$, and (d) $3.2\times10^{10}\lambda$.

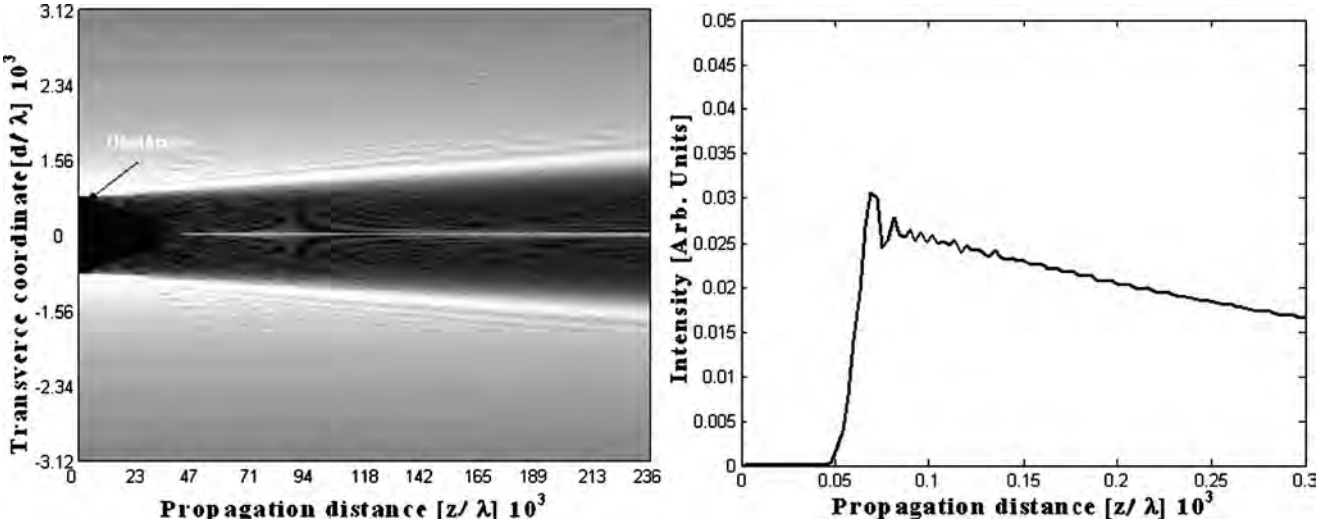

Fig. 5 Evolution of an OCW partially obstructed on axis, in the (x,z) plane, and behavior of the intensity on axis of the blocked beams.

to the fact that there is no source on axis to keep feeding the OCW. It is the diffracted shadow of a point obstruction on axis.

We can conclude from the previous analysis that the behavior of the intensity distribution just behind the circular obstruction illuminated with an ICW and OCW depends on where it was placed. When the obstruction was on axis, the edge waves contributed to the formation of the well-known Poisson ring distribution, which appeared at the same position for both kinds of waves.[21] When using a plane wave to illuminate the obstruction, the Arago spot appeared at the same plane, confirming that, for the ICWs and OCWs, it is due to the edge waves and independent of the cone of wave vectors. Further, if the obstruction was illuminated with an ICW beyond the geometric shadow, a nondiffracting Bessel beam was created. For both conical waves, when the obstruction was set off axis, the Poisson ring distribution was not observed within the shadow area, but an interference pattern was observed instead; this is due to the edge waves presenting different amplitude and phase along the circumference of the obstruction.

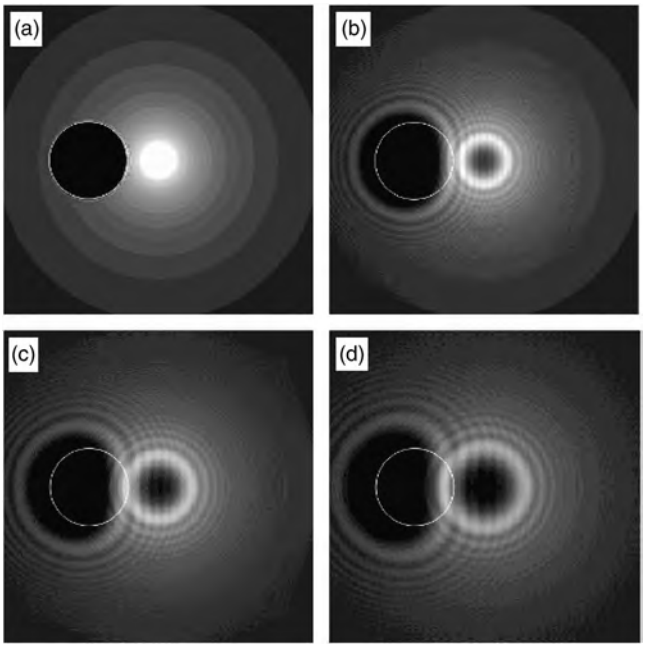

Fig. 6 Dynamics of an OCW partially blocked off axis. Distance from the obstruction: (a) $15\times10^4\lambda$, (b) $4.7\times10^4\lambda$, (c) $9.4\times10^4\lambda$, and (d) $1.4\times10^5\lambda$.

4 Numerical Simulations of Partially Obstructed Bessel Beams

Considering that Bessel beams are formed by the superposition of ICWs and OCWs, the analysis in the previous section provides what is necessary to understand the patterns observed when an obstruction was placed in the path of a Bessel beam.

From the typical arrangements to generated Bessel beams we can note the following features:

1. Bessel beams generated by a mask and a lens have two important zones. In one of them, both conical waves exist [see Fig. 2(a)], and in the other only outgoing waves are present [see in Fig. 2(a)].
2. Generation of Bessel beams with an axicon presents three zones: in the first only incoming waves exist [see in Fig. 2(b)], in the second both conical waves are simultaneously present [see in Fig. 2(b)], and in the last only outgoing conical waves exist [see in Fig. 2(b)].

Then, depending on where the obstruction is set, different propagation dynamics will be observed.

The numerical simulations of partially obstructed Bessel beams were performed considering a Bessel function as initial condition, which produced a central lobe with a diameter of 100 μm, and a circular opaque obstruction with a diameter of 1 mm. The obstruction, placed on axis, blocked the first six rings of the beam. The dynamics of the propagation after the obstruction allowed observing a convergent

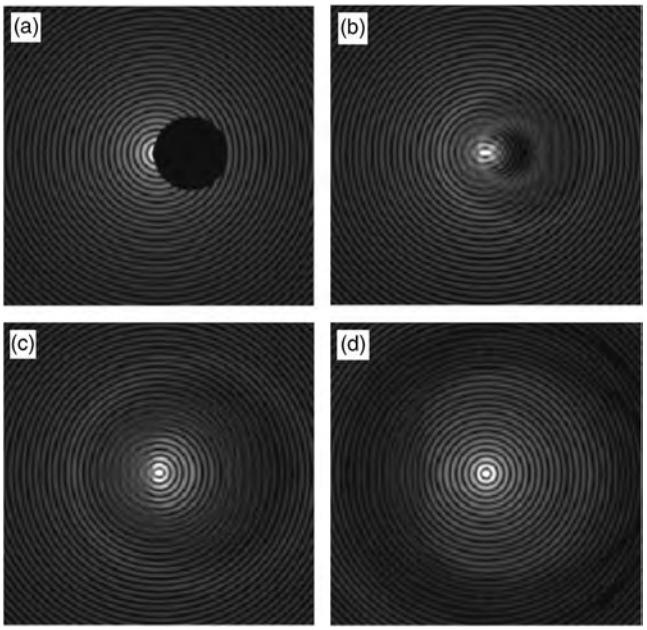

Fig. 7 Bessel beam partially blocked, from the central lobe outward, by a 1-mm circular opaque obstruction: (a) initial condition, (b) at 8 cm from the obstacle, (c) at 30 cm from the obstacle, and at (d) 45 cm from the obstacle.

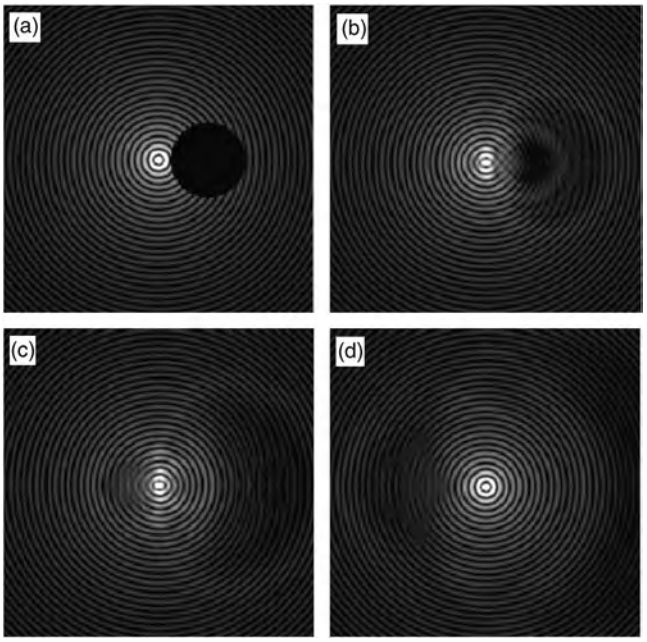

Fig. 8 Bessel beam partially blocked, from the second ring outward, by a 1-mm circular opaque obstruction: (a) initial condition, (b) at 8 cm from the obstacle, (c) at 30 cm from the obstacle, and (d) at 45 cm from the obstacle.

shadow clearly, within which also appeared the Arago spot, which was overcome by the reconstructed Bessel beam. Also, a reduction in contrast of the outer rings was observed, showing the presence of the outgoing conical shadow. With the same conditions but with the obstruction set off axis, the dynamics allowed the clear observation of two shadows, one due to the ICW and the other to the OCW.

To illustrate the dynamics of the partially blocked Bessel beam, we select two examples where the obstruction was set off axis. In the first example, the central lobe was obstructed by the circular opaque object; see Fig. 7(a). At 8 cm from the obstruction two circular shadows appeared [see Fig. 7(b)]: one larger, with low contrast, and the other smaller, with high contrast. The smaller shadow was surrounded by a bright ring and in the inner region presented an interference pattern. The rings inside the larger shadow exhibited some distortion. On increasing the distance from the obstruction, the observed larger shadow became almost circular and its diameter also increased; the smaller shadow, which was moving towards the axis, merged with the larger one after passing through the axis. At 45 cm of propagation, the central region of the Bessel beam was practically recovered, and it was surrounded by a low-contrast dark ring; see Fig. 7(d).

The other example, selected because it shows different details of the dynamics of propagation, considered the Bessel beam blocked from the second ring. The behavior obtained was the following: At 8 cm from the obstacle two circular shadows appeared, the larger with low contrast and the smaller with high contrast (see Fig. 8). The smaller shadow presented a dark region with an interference pattern of curved fringes. As in the previous case, the larger shadow did not present circular symmetry. At 30 cm, it was possible to see two shadows on opposite sides of the central lobe of the Bessel beam; the low-contrast smaller shadow had passed to the left side. The larger shadow traveled to the right, away from the center of the beam. At 45 cm from the obstacle, the larger shadow was far from the sampled region of the Bessel beam. The smaller shadow with low contrast began to increase in size and moved to the left, away from the center of the Bessel beam; see Fig. 8(d).

The effect described previously can be better analyzed by considering the intensity profiles of the transverse distribution at different propagation distances. For an example, we chose the second initial condition: when the obstruction blocks from the second ring outward (Figs. 9 and 10).

There are two interesting behaviors, so we present the analysis divided into two regions. First we present the left side of the Bessel beam from the distribution, in Fig. 9, where at $z=1$ cm it is possible to see the perturbation moving to the left, at $z=8$ cm there are many rings affected in their maximum intensity; the central lobe of the Bessel beam decays almost to half of its maximum intensity [Fig. 9(b)].

At $z=30$ cm we can see that the central lobe of the Bessel beam had practically recovered. There was a small perturbation in the distant rings [Fig. 9(c)]. The right side of the distribution followed a similar behavior (Fig. 10): the perturbation began to move to the right, at $z=8$ cm the closer rings were reduced to the half of their peak intensity, and at $z=30$ cm the rings at a distance of 5 times the initial position of the obstruction were affected.

As is seen from the previous results, the intensity on axis was affected as the blocked Bessel beam propagated. In Fig. 11 we present the behavior of the on-axis intensity for a Bessel beam under different conditions. In free propaga-

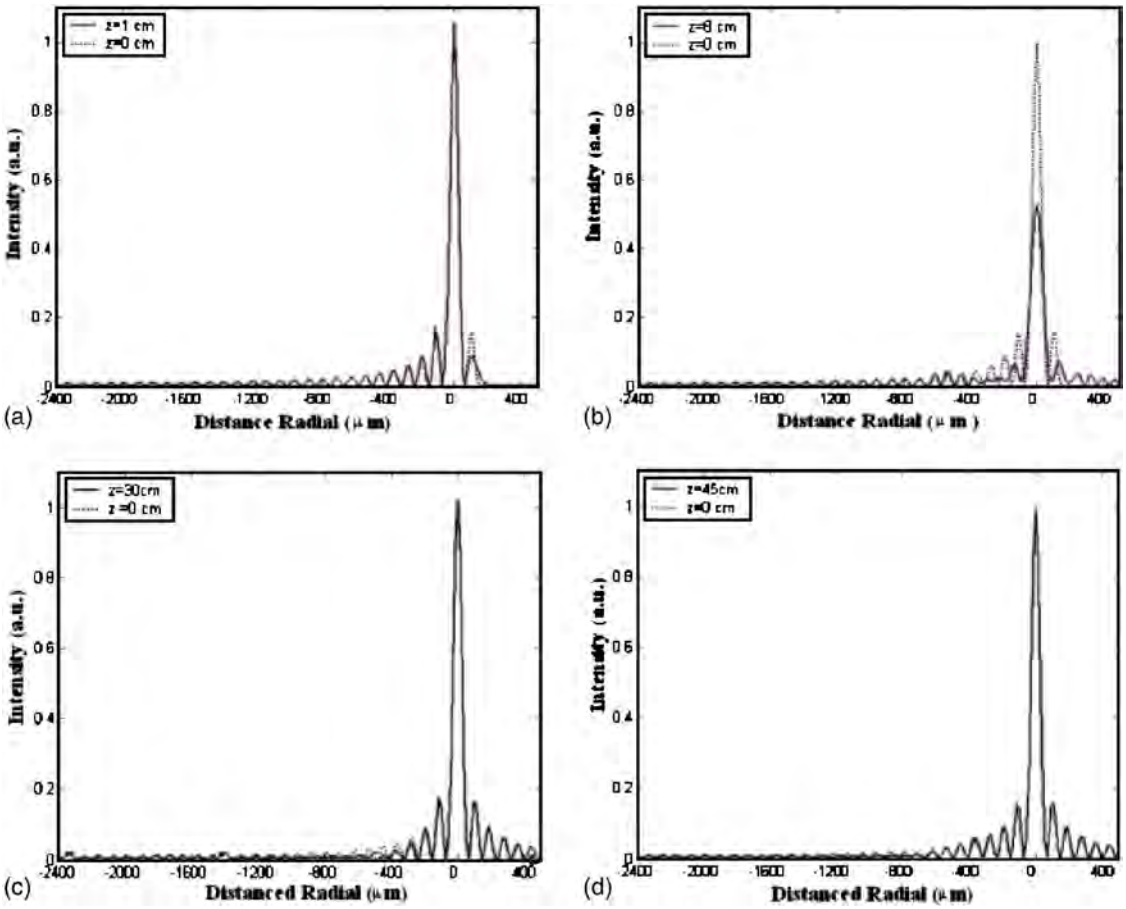

Fig. 9 Intensity profiles at different distances from the obstruction: left region. Distance of propagation: (a) 1 cm, (b) 8 cm, (c) 30 cm, and (d) 45 cm.

tion the on-axis intensity of the beam is almost constant. When obstructed on axis by an opaque circular object of 1-mm radius, it displayed oscillations. The same obstruction, but now centered in the seventh ring, affected the maximum on-axis intensity over several centimeters. The beginning of the decrease of the on-axis intensity corresponds to the displacement of one of the shadows to the central part; the minimum on-axis intensity corresponds to the passage of the shadow produced by the OCW over the main lobe of the Bessel beam (at 6 cm beyond the obstacle). Later, almost a constant on-axis intensity was recovered because the shadows moved away from the central part. Considering now a smaller obstruction, of 0.5-mm radius, set at the same position as in the previous case, the on-axis intensity follows the same behavior, with the exception that the reduction of the on-axis intensity was smaller. Also because the obstruction was farther out (radially) than in the previous case, the distance where the on-axis intensity reached its minimum was around 10 cm.

5 Experimental Configurations

Zero-order Bessel beams were generated using an annular aperture with a lens. We used a mask with thin annular ring placed at the focal length of a positive lens. This mask was illuminated with monochromatic beam from a He-Ne laser (30 mW) at $\lambda = 633$ nm, which was expanded to a diameter of 10 mm using a microscope objective and a lens. The diameter of the annular slit was 2 mm. This mask was placed at the back focal plane of a positive lens of 35-cm focal length and 2.5-cm diameter. After the lens the Bessel beam was formed. Under these conditions the maximum distance, $Z_{\max}$, for which the Bessel beam exist is given by[22,23]

$$Z_{\max} = \frac{R_L f}{r_a}, \tag{4}$$

where r_a is the radius of the annular aperture, and R_L and f are the radius and focal length of the lens, respectively. With our experimental condition the distance was around 4 m. The central lobe of the generated Bessel beam had a diameter of approximately 80 μm.

Another way to produce Bessel beams is with an axicon.[24] The axicon is a cone made with a material of refractive index n, with the property of deviating the incoming rays towards the optical axis by the same angle [$\beta = (n-1)\alpha$ where α is the angle of the axicon]. The dimensions of the axicon and its angle α determine the maximum distance $Z_{\max}$ over which the Bessel beam can be considered as invariant. We used an axicon of 2.5-cm diameter with an angle $\alpha = 0.5$ deg $= 8.72 \times 10^{-3}$ rad and refractive index $n = 1.5$. When the axicon was illuminated

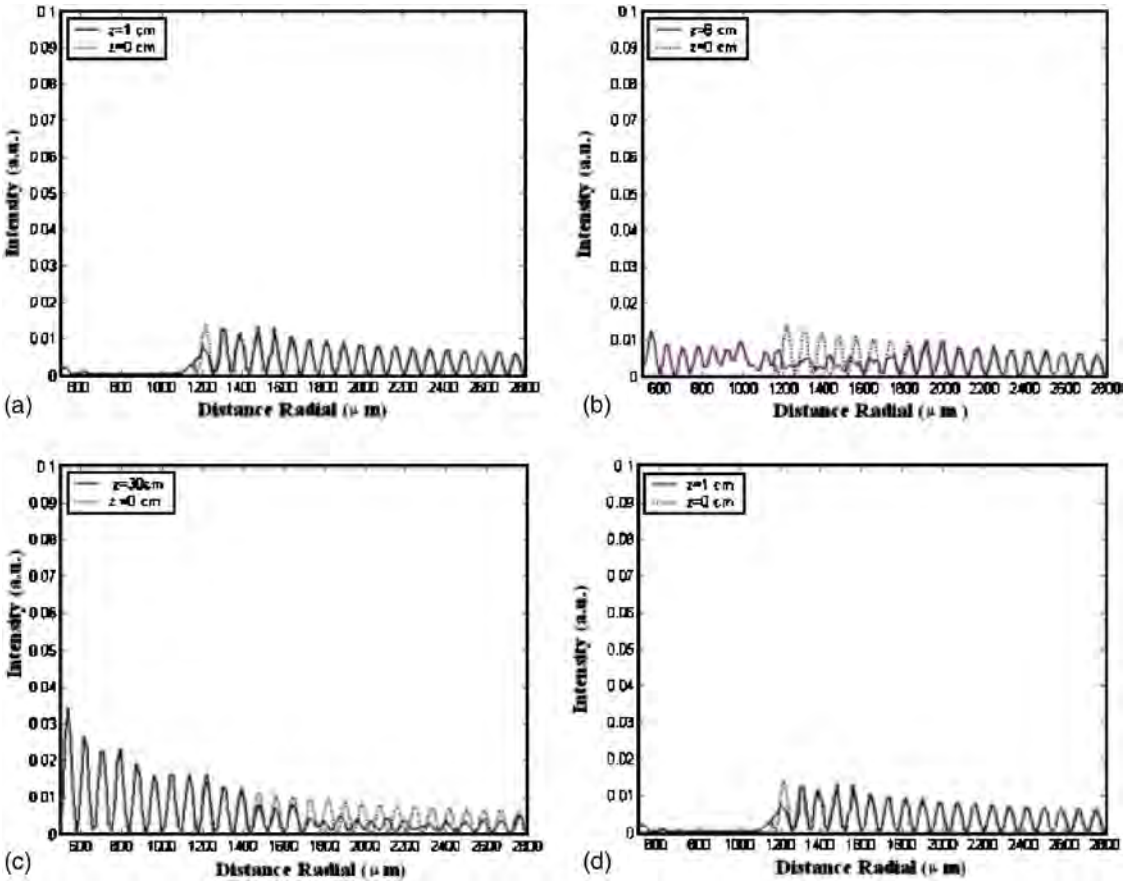

Fig. 10 Intensity profiles at different distances from the obstruction: right region. Distance of propagation: (a) 1 cm, (b) 8 cm, (c) 30 cm, and (d) 45 cm.

with a wave plane, an invariant Bessel distribution was obtained over a distance of about of 2.7 m. Within this distance the number observed rings increased, reaching a maximum, and then decreased as expected; See Fig. 2.

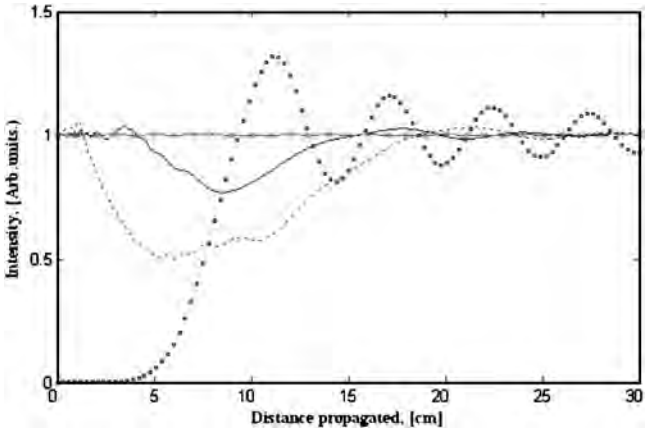

Fig. 11 On-axis intensity for a Bessel beam: free (solid line, (×)); obstructed off axis by a circular opaque object of diameter 1 mm (dashed line) and 0.5 mm (solid line), both centered on the seventh ring; obstructed on axis by a circular opaque object of diameter 1 mm (squares).

6 Experimental Results

We present the evolution of a Bessel beam generated by an annular mask and a positive lens when it was obstructed by a circular opaque object. We set the obstacle off axis at the same positions as those of the simulations discussed in the preceding section; see Fig. 12. In the first case, Fig. 12(a), the obstruction blocked the central lobe of the Bessel beam, and in the second case, Fig. 12(b), it blocked the second ring.

In both cases two circular shadows were generated. The

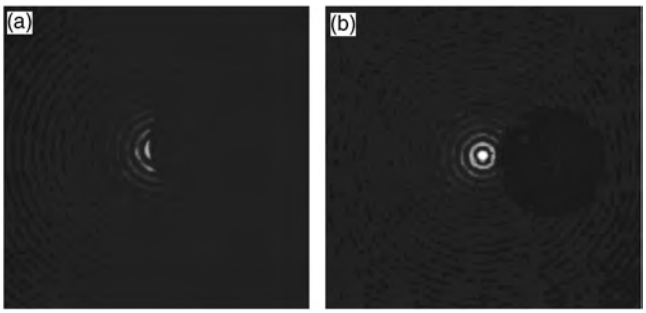

Fig. 12 Bessel beam partially blocked by a circular opaque object of 1-mm diameter from (a) the main lobe and (b) the second ring outward.

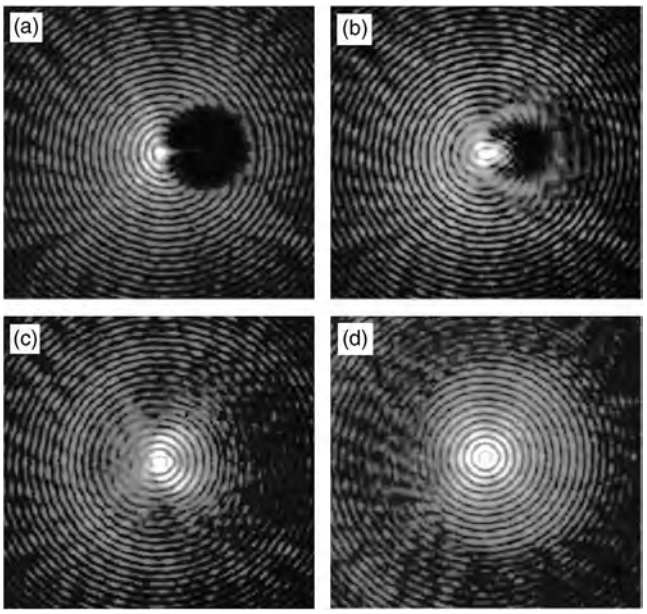

Fig. 13 Bessel beam partially blocked, by 1-mm circular opaque obstruction, form the central lobe outward: (a) initial condition, (b) at 8 cm from the obstacle, (c) at 30 cm from the obstacle, and (d) at 45 cm from the obstacle.

larger shadow was not well defined; the smaller shadow was surrounded by a bright ring [see Figs. 13(b) and 14(b)]. On increasing the distance from the obstacle, the larger shadow grew and moved farther from the center, while the smaller shadow decreased in diameter and appeared on the opposite side.

At 30 cm the difference between the two conditions is that in the second case [Fig. 14(c)] two shadows are observed on opposite sides of the central lobe, while in the first case [Fig. 7(c)] a circular shadow was observed surrounding the central spot. At a distance of 45 cm, the Bessel beam was practically regenerated. The on-axis intensity after a distance of 25 cm recovered its constant value. As comparison for the dynamics of obstructed Bessel beams when the obstruction is set on axis, we present the results obtained with the axicon; see Fig. 15. The obstruction was set on axis at a distance of 30 cm from the axicon. In this case, the convergent shadow is clear. The divergent shadow had low contrast and overlapped the outer rings, so that it is difficult to distinguish. Note, however, that the frequency of the rings inside the shadow was affected. From the experimental results we can say that the presence of the ICW and OCW was evident from the different shadows produced when the Bessel beams was obstructed by an opaque object. The divergent shadow was due to the OCW, and the convergent shadow to the ICW.

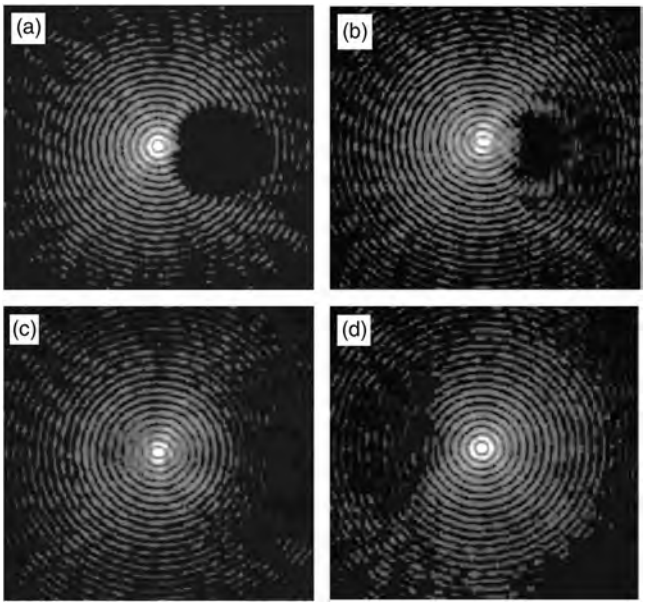

Fig. 14 Bessel beam partially blocked, by 1-mm circular opaque obstruction, from the second ring outward: (a) initial condition, (b) at 8 cm from the obstacle, (c) at 30 cm from the obstacle, and (d) at 45 cm from the obstacle.

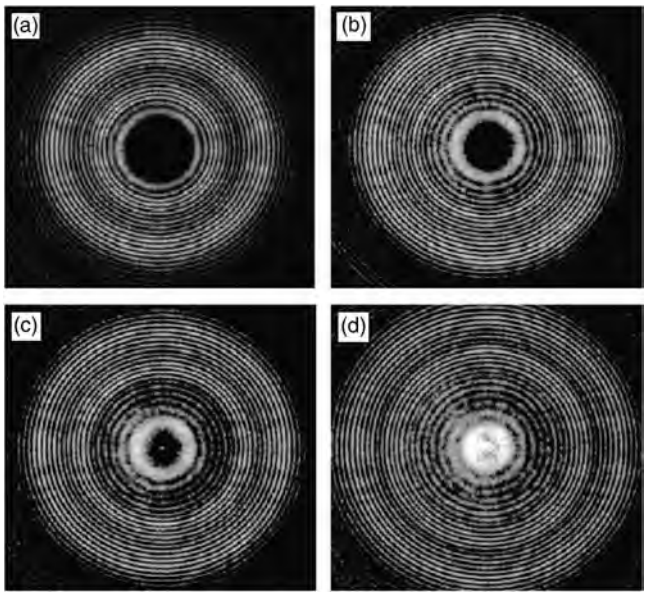

Fig. 15 Bessel beam blocked on axis: (a) 1 cm, (b) 3 cm, (c) 6 cm, and (d) 9 cm from the obstruction.

7 Conclusions

We investigated the behavior of individual conical waves when they are partially obstructed by opaque objects. In the case of outgoing conical waves a divergent shadow was obtained without regard to the position of the obstruction. In the case of an incoming conical wave a convergent shadow appears. For an obstruction off axis, the shadow moves towards the optical axis and then appears on the other side of it, but now as a divergent shadow. The shape and size of the object affect the transverse distribution but not the general dynamics of the shadows.

These results, applied to the case of Bessel beams, indicate that, depending on the position, size, and form of the opaque object, which affect the individual conical waves, the invariance or adiffractionality of these beams may be lost. Experimental results with partially obstructed Bessel beams showed the formation of two shadows, one due the ICW and the other to the OCW. The dynamics of the shad-

ows depended on the position of the obstruction. Our theoretical and experimental results show that the energy of finite Bessel beams appears to travel parallel to the optical axis. However, the energy flux in fact follows the direction dictated by the cone of wave vectors of its constituent ICW and OCW.

References

1. J. Lu and J. F. Greenleaf, "Diffraction-limited beams and their applications for ultrasonic imaging and tissue characterization," *Proc. SPIE* **1733**, 92–119 (1992).
2. R. M. Herman and T. A. Wiggins, "Productions and uses of diffraction less beams," *J. Opt. Soc. Am. A* **8**, 932–942 (1999).
3. V. Garcés-Chávez, D. McGloin, H. Melville, W. Sibbett, and K. Dholakia, "Simultaneous micromanipulation in multiple planes using a self-reconstructing light beam," *Nature (London)* **419**, 145–147 (2002).
4. V. Garcés-Chávez, D. McGloin, M. D. Summers, A. Fernandez-Nieves, G. C. Spalding, G. Cristobal, and K. Dholakia, "The reconstruction of optical angular momentum after distortion in amplitude, phase and polarization," *J. Opt. A, Pure Appl. Opt.* **6**, S235–S238 (2004).
5. J. Durnin, "Exact solutions for nondiffracting beams. I. The scalar theory," *J. Opt. Soc. Am. A* **4**, 651–654 (1986).
6. K. Dholakia, H. Little, C. T. A. Brown, B. Agate, D. McGloin, L. Paterson, and W. Sibbett, "Imaging in optical micromanipulation using two-photon excitation," *New J. Phys.* **6**, 136–145 (2004).
7. R. P. MacDonald, S. A. Boothroyd, T. Okamoto, J. Chrostowoski, and B. A. Syrett, "Interboard optical data distribution by Bessel beam shadowing," *Opt. Commun.* **122**, 169–177 (1996).
8. Z. Bouchal, J. Wagner, and M. Chlup, "Self-reconstruction of a distorted nondiffracting beam," *Opt. Commun.* **151**, 207–211 (1998).
9. S. H. Tao and X. Yuan, "Self-reconstruction property of fractional Bessel beams," *J. Opt. Soc. Am. A* **21**(7), 1192–1197 (2004).
10. S. Sogomonian, S. Klewitz, and S. Herminghaus, "Self-reconstruction of a Bessel beam in nonlinear medium," *Opt. Commun.* **139**, 313–319 (1997).
11. A. Dubietis, E. Kucinskas, G. Tamosauskas, and E. Gaizauskas, "Self-reconstruction of light filaments," *Opt. Lett.* **29**, 2893–2895 (2004).
12. D. DeBeer, S. R. Hartmann, and R. Friedberg, "Comment on Diffraction-free beams," *Phys. Rev. Lett.* **59**, 2611–2612 (1987).
13. S. Chavez-Cerda, G. S. McDonald, and G. H. C. New, "Nondiffracting beams: traveling, standing, rotating and spiral waves," *Opt. Commun.* **123**, 225–233 (1996).
14. S. Chavez-Cerda, "A new approach to Bessel beams," *J. Mod. Opt.* **46**(6), 923–930 (1999).
15. S. Chavez-Cerda and G. H. C. New, "Evolution of focused Hankel wave and Bessel beams," *Opt. Commun.* **181**, 369–377 (2000).
16. M. A. Porras, A. Parola, D. Faccio, A. Dubietis, and P. D. Trapani, "Nonlinear unbalanced Bessel beams: stationary conical waves supported by nonlinear losses," *Phys. Rev. Lett.* **93**, 153902 (2004).
17. M. A. Bandrés, J. C. Gutiérrez-Vega, and S. Chávez-Cerda, "Parabolic nondiffracting optical wavefields," *Opt. Lett.* **29**, 44–46 (2004).
18. J. C. Gutiérrez-Vega, M. D. Iturbe-Castillo, and S. Chávez-Cerda, "Alternative formulation for invariant optical fields: Mathieu beams," *Opt. Lett.* **25**, 1493–1495 (2000).
19. J. C. Gutierrez-Vega, M. D. Iturbe-Castillo, G. A. Ramirez, E. Tepichin, R. M. Rodriguez-Dagnino, S. Chavez-Cerda, and G. H. C. New, "Experimental demonstration of optical Mathieu beams," *Opt. Commun.* **195**, 35–40 (2001).
20. E. T. Whittaker and G. N. Watson, *A Course of Modern Analysis*, Cambridge Univ. Press, Cambridge, England (1927).
21. R. L. Lucke, "Rayleigh-Sommerfeld diffraction and Poisson's spot," *Eur. J. Phys.* **27**, 193–204 (2006).
22. J. Durnin, J. J. Miceli, Jr., and J. H. Eberly, "Diffraction-free beams," *Phys. Rev. Lett.* **58**, 1499–1501 (1987).
23. Y. Lin, W. Seka, J. H. Eberly, H. Huang, and D. L. Brown, "Experimental investigation of Bessel beam characteristics," *Appl. Opt.* **31**, 2708–2713 (1992).
24. J. H. McLeod, "The axicon: a new type of optical element," *J. Opt. Soc. Am.* **44**, 592–597 (1954).

Marcelino Anguiano-Morales graduated in physics in 1999 from Facultad de Ciencias Físico Matemáticas of the Benemérita Universidad Autónoma de Puebla, México, and his master's degree in 2002. He is a graduate student in optoelectronics. His research interests are the applications of invariant beams.

M. Maribel Méndez-Otero graduated in physics in 1995 from the Facultad de Ciencias Físico Matemáticas of the Universidad Autónoma de Puebla, México. Her master's and doctoral degrees were obtained in 1996 and 2000, respectively, in the Instituto Nacional de Astrofísica Óptica y Electrónica. She is currently working in the Facultad de Físico Matemáticas. Her research involves measurement of nonlinear absorption and refraction in solid and liquid materials. Recently she has initiated work on the propagation of invariant beams in free space. She is a full-time researcher at the BUAP.

M. David Iturbe-Castillo is a titular researcher in the optics department at INAOE. He received his PhD from the same institute in 1996. His research interests are in nonlinear optical characterization of materials and propagation-invariant beams in linear and nonlinear media.

Sabino Chávez-Cerda received his PhD degree in nonlinear optics (physics) at Imperial College of Science and Technology, University of London, Great Britain. He has been a full-time researcher at Instituto Nacional de Astrofisica Optica y Electrónica (INAOE) since January 1995. His research field is theoretical linear and nonlinear optics; he is investigating the physics of light propagation (as beams and pulses) in dispersive linear and nonlinear refractive media using analytical and numerical techniques.